THE JOURNAL OF PHYSICAL CHEMISTRY C

pubs.acs.org/JPCC Article

Heteroatom-Doped Transition Metal Nitrides for CO Electrochemical Reduction: A Density Functional Theory Screening Study

Mohammadreza Karamad,* Amir Barati Farimani, Rishikesh Magar, Samira Siahrostami, and Ian D. Gates*

Cite This: J. Phys. Chem. C 2020, 124, 26344−26351 Read Online

ACCESS | Metrics & More | Article Recommendations | Supporting Information

ABSTRACT: Electrochemical reduction of CO_2 to fuels has attracted a great deal of attention in recent years as a potential solution to close the carbon cycle. In search for novel catalyst materials, we present in this study density functional theory-based screening of heteroatom-doped transition metal nitrides. We first examine zinc blend and rock salt polymorphs of transition metal nitrides and then consider doping the surface with 25% B, P, Sb, Bi, and C heteroatoms. We fully assess the stability and activity of the examined catalysts. The catalytic activity is measured by the calculated limiting potential, and the stability is assessed against hydroxyl (*OH) poisoning as well as dissolution under CO reduction relevant potentials. Of the screened nitrides, many are predicted to be active for the CO reduction reaction but only a few are stable under electrochemical conditions. In particular, on nearly all of the metal nitrides with a desired catalytic activity for CO reduction, either the competing hydrogen evolution reaction prevails over CO reduction or *OH poisoning occurs at CO reduction onset potentials. We identify five promising candidates including P-doped NbN, C-doped VN, P-doped VN, TiN, and Sb-doped TiN. Ultimately, this study emphasizes the relevance of stability under electrochemical conditions and the importance of taking into account the competition between the CO reduction, hydrogen evolution, and *OH reduction reactions under electrochemical conditions.

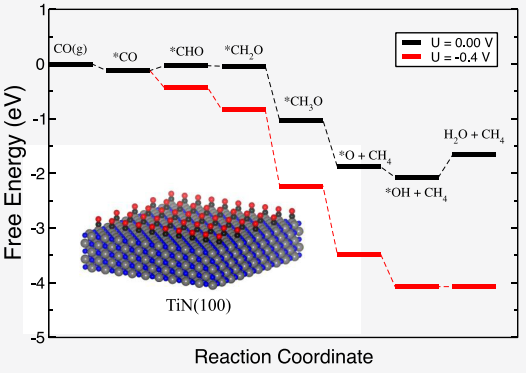

INTRODUCTION

Fossil fuels are currently the primary sources of energy and chemical products. The combustion of fossil fuels has resulted in increasing anthropogenic CO_2 emissions in the atmosphere.[1] Therefore, it is necessary to develop sustainable alternatives for long-term energy supplementation that could simultaneously address the mitigation of harmful CO_2. Electrochemical reduction of CO_2 (CO_2 RR) is a promising method to address these concerns.[2] In a carbon energy cycle, renewable energy sources such as wind or solar are used to reduce CO_2 back to valuable chemicals and fuels, such as alcohols and hydrocarbons. Depending on the catalyst material, different products may form during the CO_2 RR. Formic acid and CO are formed through two-electron−proton (2e-) reduction of CO_2. Further reduced products such as hydrocarbons and alcohols can also be formed, which require more than 2e- transfer steps. CO has been shown to be the primary intermediate in the CO_2 RR to produce any further reduced products. Therefore, many studies in the literature have directly investigated electrochemical CO reduction (CO RR) when considering CO_2 RR.[3,4] The majority of previous reports in the literature have focused on copper-containing electrocatalysts for the CO/CO_2 reduction reaction mainly because it is the only metal that shows high selectivity for hydrocarbons, mainly methane and ethylene.[5−12] However, a significantly high overpotential (∼1 V) is required to obtain a reasonable current density of several mA/cm^2 on Cu.[13,14] Thus, development of more efficient catalysts remains a challenge. From a catalysis perspective, the three main challenges of CO_2 RR are catalyst activity, stability under reducing conditions, and selectivity toward desired products.[15] Different classes of materials including carbon-based materials, metal-functionalized porphyrinlike structures, transition metal oxides, metal−organic frameworks, and transition metals embedded in graphene have been explored and have shown promise for CO_2 RR.[16−23]

Transition metal nitrides (TMNs) are particularly interesting class of materials as potential electrocatalysts due to their desired properties such as high electrical and thermal conductivities, tailorable electronic features, and chemical stability in aqueous media.[24,25] They have been examined for different electrochemical reactions such as the oxygen reduction reaction

Received: September 28, 2020
Published: November 12, 2020

https://dx.doi.org/10.1021/acs.jpcc.0c08832
J. Phys. Chem. C 2020, 124, 26344−26351

(ORR), oxygen evolution reaction (OER), reduction of nitrogen to ammonia, and hydrogen evolution reaction (HER).[26−31] However, to the best of our knowledge, they have not been examined for the CO RR or CO_2 RR. Herein, we perform a high-throughput density functional theory (DFT)-based screening of TMNs and their heteroatom-doped structures to identify viable and efficient catalysts for CO RR. We investigate both stability and activity under CO reduction conditions and competition with the HER. Our results show that many TMNs activate the CO RR but only a few are stable under relevant electrochemical conditions. We show that the stability of the catalysts against hydroxyl poisoning and dissolution at relevant CO reduction potentials or the competing HER is the main issue.

COMPUTATIONAL DETAILS

DFT calculations using the QUANTUM ESPRESSO package were conducted to determine the adsorption energies of various adsorbates.[32] The Perdew−Burke−Ernzerhof (PBE) functional was used as the exchange−correlation functional.[33] The ion−electron interaction is described by ultrasoft pseudopotentials.[34] For bulk metal nitrides, Kohn−Sham wave functions were expanded in a series of plane waves with a converged energy cutoff of 550 eV and a density cutoff of 5500 eV. The rock salt and zinc blend surfaces were modeled using five-layer slabs consisting of 24 and 40 atoms, respectively, repeated in a supercell geometry with at least 17 Å of vacuum between successive slabs. Adsorption was allowed only on one side of the slabs. In all calculations, the bottom two layers were fixed in their bulk structure, whereas the top three layers and adsorbates on them were allowed to relax in all directions. We used a Monkhorst−Pack grid with dimensions of $4 \times 4 \times 1$ for sampling the first Brillouin zones.[35] All adsorption sites were considered and only the most stable ones are reported here. The final structures after relaxation were checked, and the ones with surface reconstruction, where a surface atom or an adsorbate displaces more than 3 Å, were excluded from further analysis. The binding energies of all adsorbates studied in this work are provided in the Supporting Information.

The computational hydrogen electrode method introduced by Nørskov et al.[36] was used to calculate the free energy levels of all adsorbates. In this model, the free energy change of each electrochemical reaction step that involves an electron−proton transfer is calculated using the reversible hydrogen electrode (RHE), where the chemical potential of an electron−proton pair is equal to that of half of hydrogen in the gas phase under standard conditions. The electrode potential is taken into account by shifting the electron energy by −eU where e and U are the elementary charge and the electrode potential, respectively. The limiting potential is defined as the negative of the maximum free energy difference between any two successive electrochemical steps.

RESULTS AND DISCUSSION

We start by modeling CO reduction since CO is an inevitable intermediate in CO_2 reduction to hydrocarbons or alcohols. Moreover, CO adsorption could promote CO reduction selectivity toward desired products by suppressing the competing HER due to the site blocking effect and/or changes in the adsorbed hydrogen (*H) binding energy. We consider mononitrides consisting of d-block transition metals (a pool of 21 elemental metals) including NiN, CoN, RuN, RhN, IrN, FeN, PdN, and OsN with a zinc blend crystal structure and MnN, YN, VN, ScN, CrN, HfN, MoN, ZrN, and TaN with a rock salt crystal structure. We only focus on the low index facets of (100) and (110) for rock salt and zinc blend structures, respectively.[31] In addition, we investigate the catalytic activity and stability of metal nitrides by introducing heteroatom dopants.[37] To explore the doping effects, we examined 25% of the surface atoms doped by five different heteroatoms including B, P, Sb, Bi, and C. Figure 1 shows the snapshots of undoped TiN(100), C-doped TiN(100), undoped CoN(110), and C-doped CoN(110) as examples of screened catalysts.

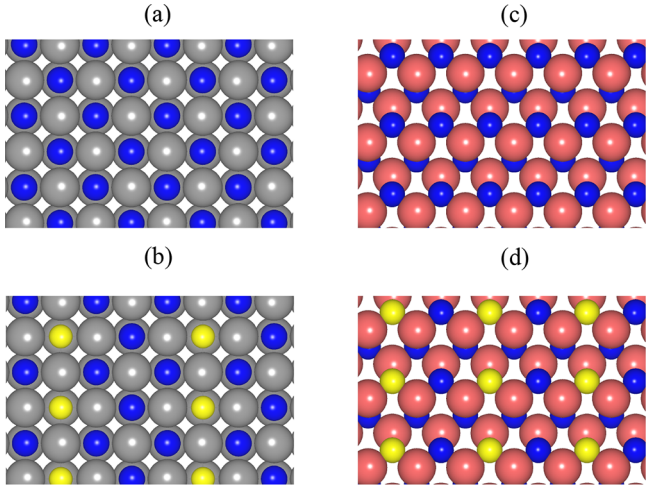

Figure 1. Top views of (a) undoped TiN(100), (b) C-doped TiN(100), (c) undoped CoN(110), and (d) C-doped CoN(110). TiN and CoN have zinc blend and rock salt crystal structures, respectively. Dark blue, yellow, pink, and gray atoms are N, C, Co, and Ti sites, respectively.

We follow three steps in our computational screening study. First, we define a set of descriptors to assess the catalytic activity of the metal nitrides under electrochemical CO reduction potentials. Second, we define a set of descriptors to assess the stability of the metal nitrides under electrochemical conditions. In this step, we include *OH and *H binding energies and metal nitride dissolution potentials obtained from DFT calculations. Finally, we select the metal nitrides with the highest predicted catalytic activity and stability for further analysis. We will discuss each of these steps in more detail in the following sections.

Descriptors for CO Reduction. We focus on calculating the thermodynamic adsorption energies of intermediates, which is the first step in computational catalyst screening. This analysis provides a mechanistic insight as well as guidance on the design and optimization of different catalysts. Further analysis of the activation energies is required for the most promising candidates to estimate the turnover frequency, which is outside the scope of this study.

Previous electronic structure calculations have shown that the reduction of *CO to *CHO is the potential limiting step in the CO reduction on Cu and late transition metals.[14,38,39] The theoretical limiting potential for the catalyst materials that bind CO is defined as

$$U_L = -(\Delta G_{*CHO} - \Delta G_{*CO})/e \quad (1)$$

where ΔG_{*CHO} and ΔG_{*CO} are the binding free energies of *CO and *CHO, respectively, and e is the electron charge. Previous reports demonstrated a close agreement between the theoretical

https://dx.doi.org/10.1021/acs.jpcc.0c08832
J. Phys. Chem. C 2020, 124, 26344−26351

overpotential and the experimental onset potential for CO_2 reduction on Cu.[14,39,40] For the catalyst materials that do not bind CO, the rate of CO desorption is high and CO is the major product. Therefore, the following reaction is considered for CO reduction

$$* + CO(g) + (H^+ + e^-) \rightarrow *CHO \quad (2)$$

and the corresponding theoretical limiting potential is defined as

$$U_L = -(\Delta G_{*CHO} - \Delta G_{CO(g)})/e \quad (3)$$

where $\Delta G_{CO(g)}$ is the chemical potential of CO in the gas phase. The potential limiting step for CO reduction on metal nitrides could, in principle, be different from the one for pure metals. However, in the first step, we take the same potential limiting step as that of pure metals, which provides the lower limit in the CO reduction reaction catalytic activity. Of note, CO reduction could occur through *COH formation rather than *CHO. Recent DFT calculations show that the formation of *CHO is thermodynamically more favored over *COH on Cu(111) and step sites of the late transition metals. On the other hand, according to a recent study by Nie et al.,[41] formation of *CHO is less favorable than *COH when the kinetic barriers for proton transfer to adsorbed CO and surface hydrogenation in the presence of water molecules are considered. Herein, we consider both *CHO and *COH formation in our screening study. We find that on nearly all TMNs, *CHO binds stronger than *COH. As will be discussed in the following sections, on all promising TMN catalysts that survive the activity and stability criteria, *CHO is more stable than *COH. We note that a thorough mechanistic study that includes kinetic barriers may be required to determine the full CO reduction pathway on TMNs.[20,38] However, thermodynamics based on the binding energies of CO* and CHO* is a necessary step, which is why we emphasize on them in this work. Figure 2 shows the binding

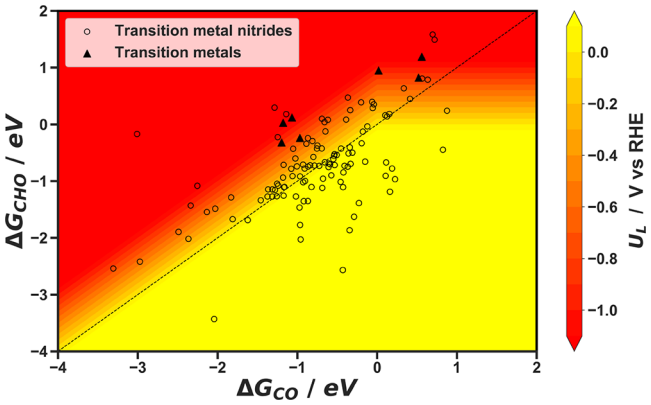

Figure 2. Contour plot of the calculated limiting potential for *CO/CO(g) reduction to *CHO using eqs 3 and 4 for the studied metal nitrides in this work (circles). Similar data for the (111) facets of bare transition metals are provided for comparison (triangles).

energies of *CHO versus *CO on our examined TMNs. The data for pure transition metals (111) are also shown for comparison. The color bar shows the limiting potential for *CHO formation, defined based on eq 1 and eq 3. The yellow region is the region of interest with a minimum overpotential and a maximum activity. An ideal catalyst with a zero overpotential has similar binding energies for *CO and *CHO, which means that the formation of *CHO is thermoneutral. However, as shown in Figure 2, this is not the case for any of the transition metals, consistent with the associated high overpotentials required for CO reduction.[14] In contrast, many of the TMNs are in the region with a low overpotential, and interestingly, the binding energies of *CO and *CHO are scattered. There are even many metal nitrides for which the formation of *CHO from *CO is exergonic in energy. Care, however, should be taken when defining the CO RR catalytic activity on these TMNs. Although CHO* formation is not the rate-limiting step, one of the following sequential steps might limit CO reduction to targeted products. Therefore, we excluded TMNs that exhibit stronger binding for *CHO than that for *CO. Moreover, in this study, we are only interested in metal nitrides that exhibit a higher catalytic activity for CO reduction than that of Cu. Therefore, the metal nitrides for which the theoretical limiting potential is below −0.5 V (RHE) are eliminated from further analysis.

Previous experimental studies have shown that the activity of transition metals with a weak CO binding energy is limited by the lack of CO coverage, which ultimately limits the generation rate of CO reduction products and results in CO(g) as the main reaction product.[13,14] On the other hand, transition metals that bind CO too strongly will be poisoned by this intermediate.[14] Therefore, in line with the Sabatier principle, catalysts with moderate CO binding energies catalyze CO reduction to further reduced products.[42] In agreement with these experimental findings, a follow-up DFT study by Nørskov et al.[43] on transition metals showed that on stepped sites, which dominate the overall catalytic activity for the CO_2 reduction reaction, substantial selectivity toward CO reduction products only occurs for catalysts with CO binding energies around that of Cu. In light of these findings, we only consider metal nitrides with moderate CO binding energies of $-1 < \Delta G_{*CO} < 0$ for further consideration. Figure 3 shows the heatmaps for CO binding energies and the difference between free energies of adsorption of *CHO and *CO adsorbates, $\Delta G_{*CHO} - \Delta G_{*CO}$, for metal nitrides before and after applying the above criteria.

Stability Analysis. Next, the stability of the most promising TMNs with a favorable *CO to *CHO adsorption energy is analyzed.[44,45] We first examine *OH poisoning, which may occur due to the presence of oxophilic elements on the surfaces of metal nitrides, which facilitate water decomposition. In addition, reduction of *OH to water is one of the intermediate steps in the reaction free energy diagram of CO reduction.[38] Therefore, if *OH binds too strongly to the surface, its reduction to water becomes the potential limiting step rather than *CO reduction to *CHO. Although the presence of oxophilic elements may help to stabilize *CHO relative to *CO, it should not bind *OH too strongly.[39] The *OH reduction to water and its corresponding limiting potential are defined as

$$*OH + e^- + H^+ \rightarrow H_2O(l) + * \quad (4)$$

$$U_L = -(\Delta G_{*OH})/e \quad (5)$$

where ΔG_{*OH} is the binding free energy of *OH. Figure 4a shows the limiting potential for *OH reduction to water versus the limiting potential for *CO reduction to *CHO. To avoid *OH poisoning, *OH reduction should occur at less negative potentials than *CO reduction. For the metal nitrides that lie above the diagonal, *OH has already been reduced to water at the potentials required to reduce *CO to *CHO, so *OH poisoning does not occur. On the other hand, for the metal

https://dx.doi.org/10.1021/acs.jpcc.0c08832
J. Phys. Chem. C 2020, 124, 26344−26351

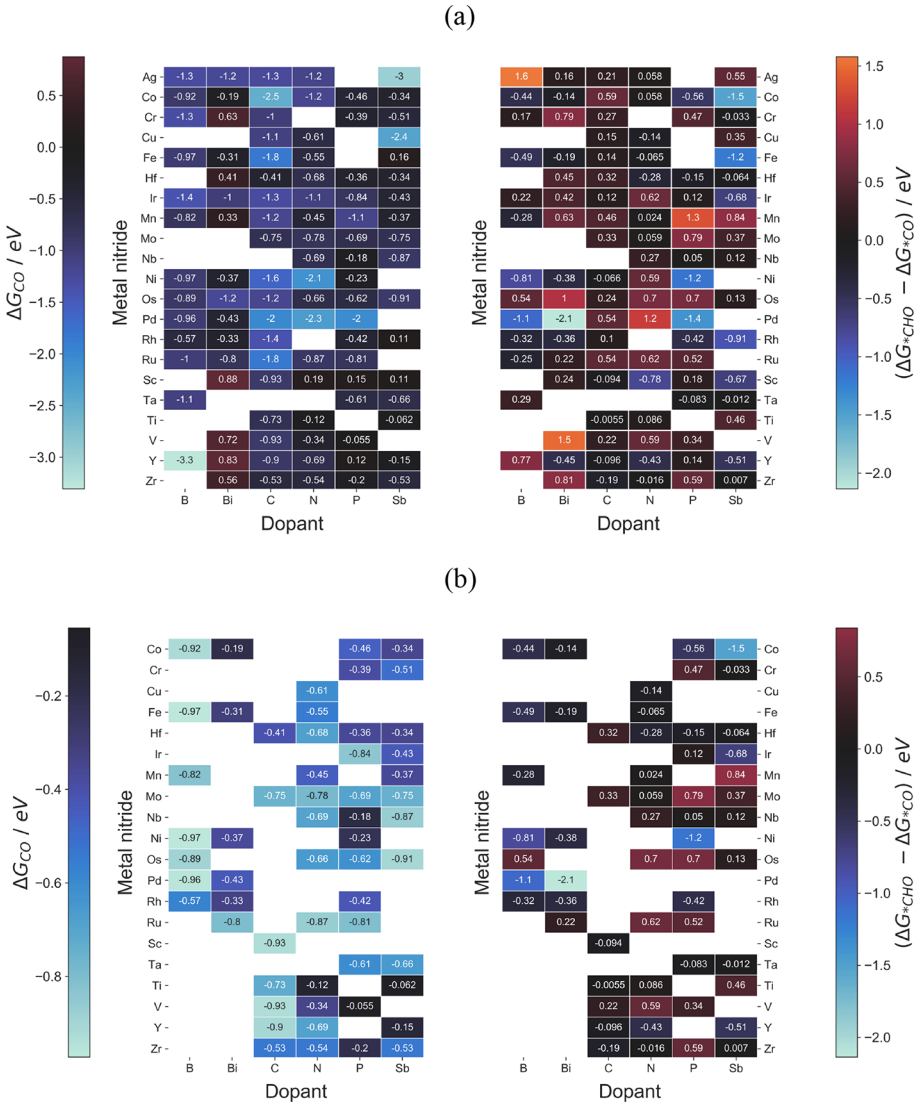

Figure 3. Heatmaps for *CO binding energies and the difference between free energies of adsorption of *CHO and *CO adsorbates, $\Delta G_{*CHO} - \Delta G_{*CO}$, for (a) all metal nitrides and (b) the ones with $-1 < \Delta G_{*CO} < 0$. The blank data correspond to the structures that underwent surface reconstruction.

nitrides that lie below the diagonal, *OH reduction takes place at more negative potentials than that required for reduction of *CO to *CHO. For these metal nitrides, *OH reduction is the potential limiting step, and an extra overpotential equal to the vertical distance to the diagonal is required to clear *OH off the surface. Figure 4b replots the data with the overall limiting potentials at which both *OH and *CO are reduced to water and *CHO, respectively. As it can be seen from Figure 4b, most of the metal nitrides with a high catalytic activity for *CO reduction suffer from *OH poisoning. This criterion excludes many potential active metal nitrides. The remaining metal nitrides are evaluated next with another stability filter, that is, dissolution.

Stability against Dissolution. The stability of the remaining metal nitrides against decomposition to metal and ammonia at working potentials is examined. We follow an approach similar to that of Abghoui and co-workers where the dissolution potential is defined as the potential at which TMNs are decomposed to ammonia and metals.[31] Figure 5 shows the dissolution potentials of promising metal nitrides as well as the corresponding working potentials for CO reduction. A metal nitride is considered stable if its dissolution potential is more negative than its corresponding CO reduction working potential.

Overall, many metal nitrides exhibit a high activity for CO reduction. Considering both activity and stability of the candidates evaluated here, given the criteria described above, there are five promising candidate metal nitrides as shown in Table 1. Among these candidates, P-doped NbN, C-doped VN, and P-doped VN are less prone to *OH poisoning and exhibit a high activity for CO reduction.

We note that our stability criteria are from a thermodynamic standpoint. Some of the metal nitrides rejected due to these stability filters might exhibit kinetic stability and remain stable under reducing conditions. For example, an element might exhibit kinetic stability, or its dissolution potential might change when doped, and consequently dissolves at higher dissolution potentials.[46] Therefore, some of the metal nitrides that failed based on the dissolution criterion might be stable under the reducing conditions. Assessing the actual stability of the metal nitrides under reducing conditions requires explicit consideration of both kinetics and thermodynamics in an exhaustive

https://dx.doi.org/10.1021/acs.jpcc.0c08832
J. Phys. Chem. C 2020, 124, 26344−26351

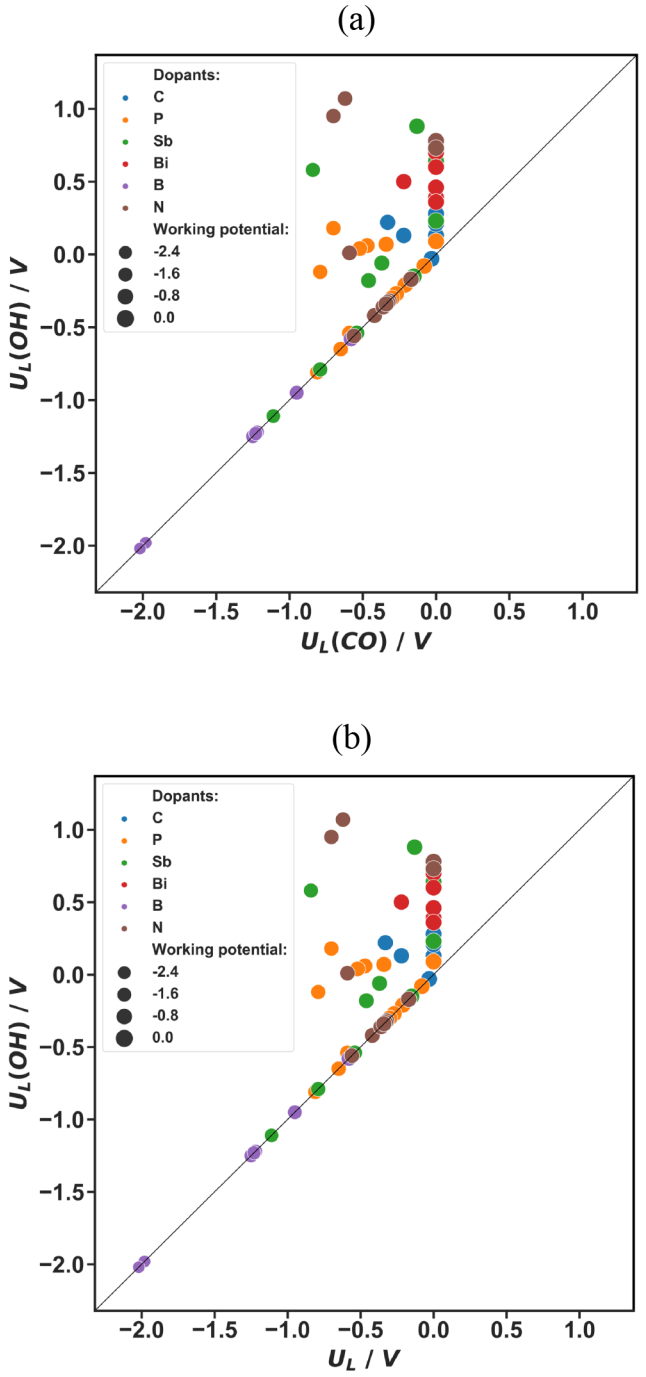

Figure 4. (a) Limiting potential for *OH reduction to water vs. the limiting potential for *CHO formation. For the points below the diagonal, *OH poisoning will prevail over *CO reduction. (b) Similar to (a), except that the points below the diagonal have been shifted vertically to the diagonal. For the metal nitrides on the diagonal, *CO and *OH reduction occurs at the same potential. The circle size corresponds to the limiting potential values. Bigger circles correspond to higher limiting potentials and vice versa. The N dopant corresponds to pure TMNs.

screening study, which is not in the scope of the current study. However, since the above stability tests capture the lower bound limit of the stability of the metal nitrides, we argue that any compound that survives these stability tests is likely to be stable under reducing conditions. Moreover, it is worth mentioning that additional compounds may become thermodynamically

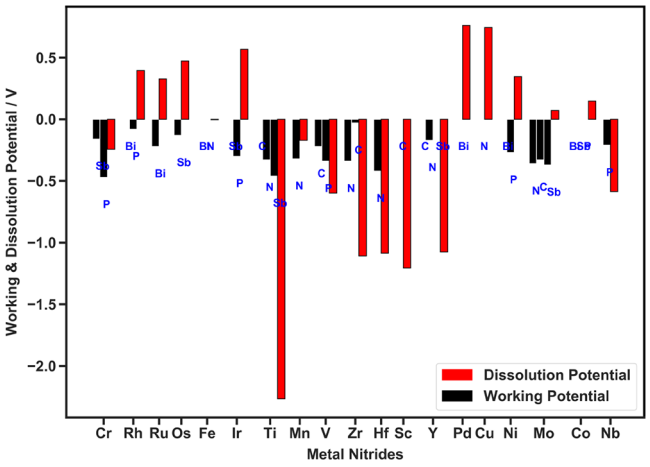

Figure 5. Dissolution and working potentials for CO reduction for promising metal nitrides. A metal nitride is considered stable if its dissolution potential is more negative than its corresponding CO reduction working potential.

stable if the CO reduction reaction occurs at higher overpotentials. In other words, improved stability could be achieved at the cost of activity. This particularly holds for compounds on which *OH poisoning occurs.

To understand the role of dopants in CO RR activity enhancement in heteroatom-doped TMNs, we compared the *CO and *CHO adsorption sites for promising doped candidates with that of undoped TMNs. It can be seen from Table 1 that for C-doped VN, P-doped VN, and Sb-doped TiN, the *CO and *CHO binding sites change. This results in changing *CO and *CHO binding energies and therefore changes in the CO RR activity.

Selectivity versus HER. Beyond the stability and activity criteria, high selectivity toward desired reaction products is a key factor in developing efficient catalysts for CO reduction. The HER is strongly competing with CO reduction at negative potentials. In reality, improving the CO reduction selectivity is contingent on suppressing the parasitic HER. The HER reaction occurs through a two-electron−proton transfer step, with *H as the only adsorbed intermediate. The binding energy of *H has been shown to be a reasonable descriptor of the hydrogen evolution activity for a wide variety of catalyst materials.[44,47] Therefore, we examine the catalytic activity of all metal nitrides toward HER by calculating the *H binding energy. It has been shown that the difference in the limiting potentials for CO_2 reduction and HER, that is, $U_L(CO) - U_L(H_2)$ follows the trends in selectivity for transition metals.[40] A more positive $U_L(CO) - U_L(H_2)$ value corresponds to a higher selectivity toward CO reduction over HER. In Figure 6, the difference in the working potentials for CO reduction and HER, that is, $U_w(CO) - U_L(H_2)$ is plotted against the working potentials for CO reduction $U_w(CO)$ for the most stable metal nitrides. In this plot, the catalysts that are in the upper-right region exhibit high activity and selectivity toward CO reduction. The results, displayed in Figure 6, suggest that P-doped NbN exhibits the highest activity for CO reduction followed by C-doped VN, TiN, P-doped VN, and Sb-doped TiN, respectively. Moreover, TiN exhibits the highest selectivity toward CO RR. We note that this statement should be taken with caution because we have investigated just two crystal terminations, namely, (100) and (110) for rock salt and zinc blend crystal structures, respectively. Since less dominant facets or defects can have different

https://dx.doi.org/10.1021/acs.jpcc.0c08832
J. Phys. Chem. C 2020, 124, 26344−26351

Table 1. List of Five Promising TMN Candidates after Considering Activity as well as Stability against *OH Poisoning and Dissolution potential[a]

TMN	Dopant	ΔG_{*CO} / eV	ΔG_{*CHO} / eV	ΔG_{*COH} / eV	U_w (CO) / V	dissolution potential / V	U_L(*OH) / V	*CO binding site	*CHO binding site
NbN	P	−0.18	−0.13	1.1	−0.21	−0.58	−0.21	Nb	Nb
VN	C	−0.93	−0.71	0.34	−0.22	−0.59	0.13	C	C
VN	P	−0.05	0.29	1.9	−0.34	−0.59	0.07	V	P
TiN	Sb	−0.06	0.4	1.2	−0.46	−2.26	−0.18	Ti	N
TiN		−0.12	0.03	2.21	−0.33	−2.26	−0.33	Ti	Ti
NbN		−0.69	−0.42	0.89	−0.55	−0.58	−0.55	Nb	Nb
VN		−0.33	0.25	1.03	−0.58	−0.59	0.01	V	V

[a]ΔG_{*CO}, ΔG_{*CHO}, and ΔG_{*COH} are the free energies of adsorption of *CO, *CHO, and *COH, respectively. U_w(CO) is the calculated working potential for *CO reduction, and U_L(*OH) is the calculated limiting potential for *OH reduction. The adsorption sites for *CO and *CHO adsorbates are provided. Similar data for undoped TMN including NbN and VN are provided for comparison.

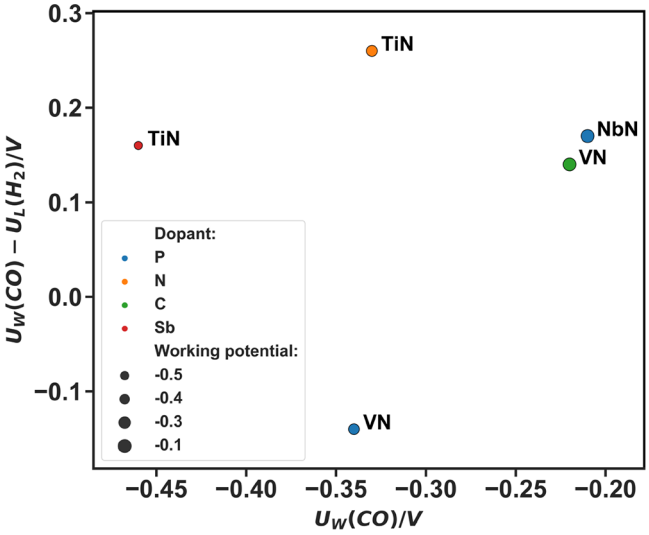

Figure 6. Differences in the working potentials for CO reduction and HER, that is, U_w(CO) − U_L(H_2) are plotted against the working potentials for CO reduction U_w(CO) for the survived metal nitrides. U_w(CO) − U_L(H_2) shows the trend in selectivity for CO reduction over HER, and U_w(CO) reflects the trend in CO reduction activity. The most promising catalysts lie on the upper-right corner of the plot. Bigger circles correspond to less negative CO reduction working potentials.

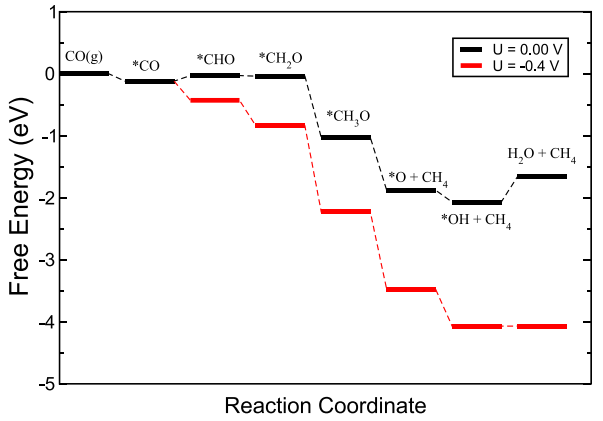

Figure 7. Free energy diagram for CO reduction on TiN(100). The black and red lines denote the free energy levels at 0 V and at working potential of −0.4 V (RHE) where all reaction steps become downhill in free energy.

selectivities and activities, it would be necessary to include other facets with different compositions in an exhaustive screening study.

Among the identified promising candidates, TiN(100) stands out as the most interesting catalyst: it exhibits highest selectivity and a moderate working potential for CO RR, that is, −0.46 V (RHE). As a comparison, on the most active step surface, Cu(211), the CO RR working potential is −0.77 V (RHE), determined using the same methodology as applied here. Moreover, as opposed to other promising candidates, it does not require doping. Therefore, we considered TiN(100) further by performing a full mechanistic pathway study to determine the final reaction product. Figure 7 shows the lowest free energy diagram (FED) pathway for CO RR on TiN(100) at zero potential and at the working potential where all electrochemical steps become downhill in free energy. The final CO RR product on TiN(100) is methane. Moreover, as initially assumed, the potential limiting step is the reduction of *CO to *CHO. However, as it can be seen from Table 1 and Figure 7, on TiN(100), the reduction of *OH to water occurs at more negative potentials. Therefore, it becomes the potential limiting step. We also note that the difference between the limiting potential for the *OH reduction value of −0.33 V (RHE) listed in Table 1 and the one in Figure 7, −0.4 V (RHE), arises from the fact that we used DFT-calculated value for H_2O+CH_4(g) free energy level in constructing the FED.

CONCLUSIONS

DFT-based screening of metal nitrides to find improved CO reduction catalysts has been conducted. We assessed the CO reduction catalytic activity of the TMNs by performing explicit DFT calculations of the binding energies of three key intermediates, namely, *CO, *CHO, and *COH. Our results show that many metal nitrides exhibit a high catalytic activity for CO reduction. However, subsequent stability tests on the metal nitrides with a high catalytic activity revealed that many of the promising candidates are unstable under CO reduction conditions. In particular, we found that *OH poisoning and metal nitride dissolution are the two main factors degrading catalyst stability. In addition, we evaluated the selectivity toward CO reduction products by taking into account the competition between CO reduction and the HER. Only metal nitrides expected to exhibit high selectivity and activity toward CO reduction products were examined. On the basis of this analysis, we predicted P-doped NbN, C-doped VN, P-doped VN, Sb-doped TiN, and TiN as the most promising candidates that exhibit simultaneous high activity, stability, and selectivity toward CO RR products. A mechanistic study on TiN(100) was performed, and it showed that methane formed as the final CO RR product. This study highlights the importance of considering

https://dx.doi.org/10.1021/acs.jpcc.0c08832
J. Phys. Chem. C 2020, 124, 26344−26351

competing reactions for the CO reduction reaction in determining the electrocatalytic activity and selectivity.

■ ASSOCIATED CONTENT

Supporting Information

The Supporting Information is available free of charge at https://pubs.acs.org/doi/10.1021/acs.jpcc.0c08832.

Free energies of adsorption of different adsorbates including *CO, *CHO, *OH, and *H on different TMNs (PDF)

■ AUTHOR INFORMATION

Corresponding Authors

Mohammadreza Karamad − *Department of Chemical and Petroleum Engineering, University of Calgary, Calgary, Alberta T2N 1N4, Canada*; Email: mohammadreza.karamad@ucalgary.ca

Ian D. Gates − *Department of Chemical and Petroleum Engineering, University of Calgary, Calgary, Alberta T2N 1N4, Canada*; Email: idgates@ucalgary.ca

Authors

Amir Barati Farimani − *Department of Mechanical Engineering, Carnegie Mellon University, Pittsburgh, Pennsylvania 15213, United States*; orcid.org/0000-0002-2952-8576

Rishikesh Magar − *Department of Mechanical Engineering, Carnegie Mellon University, Pittsburgh, Pennsylvania 15213, United States*

Samira Siahrostami − *Department of Chemistry, University of Calgary, Calgary, Alberta T2N 1N4, Canada*; orcid.org/0000-0002-1192-4634

Complete contact information is available at: https://pubs.acs.org/10.1021/acs.jpcc.0c08832

Notes

The authors declare no competing financial interest.

■ ACKNOWLEDGMENTS

The authors acknowledge support from the University of Calgary's Canada First Research Excellence Fund program and the Global Research Initiative in Sustainable Low Carbon Unconventional Resources.

■ REFERENCES

(1) Lewis, N. S.; Nocera, D. G. Powering the Planet: Chemical Challenges in Solar Energy Utilization. *Proc. Natl. Acad. Sci. U. S. A.* **2006**, *103*, 15729−15735.

(2) Gattrell, M.; Gupta, N.; Co, A. Electrochemical Reduction of CO_2 to Hydrocarbons to Store Renewable Electrical Energy and Upgrade Biogas. *Energy Convers. Manage.* **2007**, *48*, 1255−1265.

(3) Wang, L.; Nitopi, S. A.; Bertheussen, E.; Orazov, M.; Morales-Guio, C. G.; Liu, X.; Higgins, D. C.; Chan, K.; Nørskov, J. K.; Hahn, C.; et al. Electrochemical Carbon Monoxide Reduction on Polycrystalline Copper: Effects of Potential, Pressure, and PH on Selectivity toward Multicarbon and Oxygenated Products. *ACS Catal.* **2018**, *8*, 7445−7454.

(4) Schouten, K. J. P.; Pérez Gallent, E.; Koper, M. T. M. Structure Sensitivity of the Electrochemical Reduction of Carbon Monoxide on Copper Single Crystals. *ACS Catal.* **2013**, *3*, 1292−1295.

(5) Lim, H.-K.; Shin, H.; Goddard, W. A., III; Hwang, Y. J.; Min, B. K.; Kim, H. Embedding Covalency into Metal Catalysts for Efficient Electrochemical Conversion of CO_2. *J. Am. Chem. Soc.* **2014**, *136*, 11355−11361.

(6) Back, S.; Kim, H.; Jung, Y. Selective Heterogeneous CO_2 Electroreduction to Methanol. *ACS Catal.* **2015**, *5*, 965−971.

(7) Chan, K.; Tsai, C.; Hansen, H. A.; Nørskov, J. K. Molybdenum Sulfides and Selenides as Possible Electrocatalysts for CO_2 Reduction. *ChemCatChem* **2014**, *6*, 1899−1905.

(8) Asadi, M.; Kumar, B.; Behranginia, A.; Rosen, B. A.; Baskin, A.; Repnin, N.; Pisasale, D.; Phillips, P.; Zhu, W.; Haasch, R.; et al. Robust Carbon Dioxide Reduction on Molybdenum Disulphide Edges. *Nat. Commun.* **2014**, *5*, 4470.

(9) Li, C. W.; Kanan, M. W. CO_2 Reduction at Low Overpotential on Cu Electrodes Resulting from the Reduction of Thick Cu_2O Films. *J. Am. Chem. Soc.* **2012**, *134*, 7231−7234.

(10) Feng, X.; Jiang, K.; Fan, S.; Kanan, M. W. Grain-Boundary-Dependent CO_2 Electroreduction Activity. *J. Am. Chem. Soc.* **2015**, *137*, 4606−4609.

(11) Cole, E. B.; Lakkaraju, P. S.; Rampulla, D. M.; Morris, A. J.; Abelev, E.; Bocarsly, A. B. Using a One-Electron Shuttle for the Multielectron Reduction of CO_2 to Methanol: Kinetic, Mechanistic, and Structural Insights. *J. Am. Chem. Soc.* **2010**, *132*, 11539−11551.

(12) Kortlever, R.; Shen, J.; Schouten, K. J. P.; Calle-Vallejo, F.; Koper, M. T. M. Catalysts and Reaction Pathways for the Electrochemical Reduction of Carbon Dioxide. *J. Phys. Chem. Lett.* **2015**, *6*, 4073−4082.

(13) Hori, Y. Electrochemical CO_2 Reduction on Metal Electrodes. In *CO2 Reduction on Metal Electrodes. Modern Aspects of Electrochemistry*; Vayenas, C. G.; White, R. E.; Gamboa-Aldeco, M. E., Eds.; Modern Aspects of Electrochemistry; Springer New York: New York, 2008; *42*, 89−189.

(14) Kuhl, K. P.; Hatsukade, T.; Cave, E. R.; Abram, D. N.; Kibsgaard, J.; Jaramillo, T. F. Electrocatalytic Conversion of Carbon Dioxide to Methane and Methanol on Transition Metal Surfaces. *J. Am. Chem. Soc.* **2014**, *136*, 14107−14113.

(15) Hori, Y.; Murata, A.; Takahashi, R. Formation of Hydrocarbons in the Electrochemical Reduction of Carbon Dioxide at a Copper Electrode in Aqueous Solution. *J. Chem. Soc., Faraday Trans.* **1989**, *85*, 2309.

(16) Tripkovic, V.; Vanin, M.; Karamad, M.; Björketun, M. E.; Jacobsen, K. W.; Thygesen, K. S.; Rossmeisl, J. Electrochemical CO_2 and CO Reduction on Metal-Functionalized Porphyrin-like Graphene. *J. Phys. Chem. C* **2013**, *117*, 9187−9195.

(17) Siahrostami, S.; Jiang, K.; Karamad, M.; Chan, K.; Wang, H.; Nørskov, J. Theoretical Investigations into Defected Graphene for Electrochemical Reduction of CO_2. *ACS Sustainable Chem. Eng.* **2017**, *5*, 11080−11085.

(18) Bhowmik, A.; Vegge, T.; Hansen, H. A. Descriptors and Thermodynamic Limitations of Electrocatalytic Carbon Dioxide Reduction on Rutile Oxide Surfaces. *ChemSusChem* **2016**, *9*, 3230−3243.

(19) Tayyebi, E.; Hussain, J.; Abghoui, Y.; Skúlason, E. Trends of Electrochemical CO_2 Reduction Reaction on Transition Metal Oxide Catalysts. *J. Phys. Chem. C* **2018**, *122*, 10078−10087.

(20) Karamad, M.; Hansen, H. A.; Rossmeisl, J.; Nørskov, J. K. Mechanistic Pathway in the Electrochemical Reduction of CO_2 on RuO_2. *ACS Catal.* **2015**, *5*, 4075−4081.

(21) Kornienko, N.; Zhao, Y.; Kley, C. S.; Zhu, C.; Kim, D.; Lin, S.; Chang, C. J.; Yaghi, O. M.; Yang, P. Metal-Organic Frameworks for Electrocatalytic Reduction of Carbon Dioxide. *J. Am. Chem. Soc.* **2015**, *137*, 14129−14135.

(22) Hinogami, R.; Yotsuhashi, S.; Deguchi, M.; Zenitani, Y.; Hashiba, H.; Yamada, Y. Electrochemical Reduction of Carbon Dioxide Using a Copper Rubeanate Metal Organic Framework. *ECS Electrochem. Lett.* **2012**, *1*, H17−H19.

(23) Hod, I.; Sampson, M. D.; Deria, P.; Kubiak, C. P.; Farha, O. K.; Hupp, J. T. Fe-Porphyrin-Based Metal-Organic Framework Films as High-Surface Concentration, Heterogeneous Catalysts for Electrochemical Reduction of CO_2. *ACS Catal.* **2015**, *5*, 6302−6309.

(24) Jiang, L.; Gao, L. Carbon Nanotubes-Metal Nitride Composites: A New Class of Nanocomposites with Enhanced Electrical Properties. *J. Mater. Chem.* **2005**, *15*, 260−266.

(25) Didziulis, S. V.; Butcher, K. D. A Perspective on the Properties and Surface Reactivities of Carbides and Nitrides of Titanium and Vanadium. *Coord. Chem. Rev.* **2013**, *257*, 93−109.
(26) Abroshan, H.; Bothra, P.; Back, S.; Kulkarni, A.; Nørskov, J. K.; Siahrostami, S. Ultrathin Cobalt Oxide Overlayer Promotes Catalytic Activity of Cobalt Nitride for the Oxygen Reduction Reaction. *J. Phys. Chem. C* **2018**, *122*, 4783−4791.
(27) Shao, M.; Chang, Q.; Dodelet, J. P.; Chenitz, R. Recent Advances in Electrocatalysts for Oxygen Reduction Reaction. *Chem. Rev.* **2016**, *116*, 3594−3657.
(28) Peng, X.; Pi, C.; Zhang, X.; Li, S.; Huo, K.; Chu, P. K. Recent Progress of Transition Metal Nitrides for Efficient Electrocatalytic Water Splitting. *Sustainable Energy Fuels* **2019**, *3*, 366−381.
(29) Xie, J.; Xie, Y. Transition Metal Nitrides for Electrocatalytic Energy Conversion: Opportunities and Challenges. *Chem. - A Eur. J.* **2016**, *22*, 3588−3598.
(30) Yan, J.; Kong, L.; Ji, Y.; Li, Y.; White, J.; Liu, S.; Han, X.; Lee, S.-T.; Ma, T. Air-Stable Phosphorus-Doped Molybdenum Nitride for Enhanced Electrocatalytic Hydrogen Evolution. *Commun. Chem.* **2018**, *1*, 95.
(31) Abghoui, Y.; Garden, A. L.; Hlynsson, V. F.; Björgvinsdóttir, S.; Ólafsdóttir, H.; Skúlason, E. Enabling Electrochemical Reduction of Nitrogen to Ammonia at Ambient Conditions through Rational Catalyst Design. *Phys. Chem. Chem. Phys.* **2015**, *17*, 4909−4918.
(32) Giannozzi, P.; Baroni, S.; Bonini, N.; Calandra, M.; Car, R.; Cavazzoni, C.; Ceresoli, D.; Chiarotti, G. L.; Cococcioni, M.; Dabo, I.; et al. QUANTUM ESPRESSO: A Modular and Open-Source Software Project for Quantum Simulations of Materials. *J. Phys. Condens. Matter* **2009**, *21*, 39.
(33) Hammer, B.; Hansen, L. B.; Nørskov, J. K. Improved Adsorption Energetics within Density-Functional Theory Using Revised Perdew-Burke-Ernzerhof Functionals. *Phys. Rev. B* **1999**, *59*, 7413−7421.
(34) Vanderbilt, D. Soft Self-Consistent Pseudopotentials in a Generalized Eigenvalue Formalism. *Phys. Rev. B* **1990**, *41*, 7892−7895.
(35) Monkhorst, H. J.; Pack, J. D. Special Points for Brillouin-Zone Integrations. *Phys. Rev. B* **1976**, *13*, 5188−5192.
(36) Nørskov, J. K.; Rossmeisl, J.; Logadottir, A.; Lindqvist, L.; Kitchin, J. R.; Bligaard, T.; Jónsson, H. Origin of the Overpotential for Oxygen Reduction at a Fuel-Cell Cathode. *J. Phys. Chem. B* **2004**, *108*, 17886−17892.
(37) Zhou, Y.; Che, F.; Liu, M.; Zou, C.; Liang, Z.; De Luna, P.; Yuan, H.; Li, J.; Wang, Z.; Xie, H.; et al. Dopant-Induced Electron Localization Drives CO_2 Reduction to C2 Hydrocarbons. *Nat. Chem.* **2018**, *10*, 974−980.
(38) Peterson, A. A.; Abild-Pedersen, F.; Studt, F.; Rossmeisl, J.; Nørskov, J. K. How Copper Catalyzes the Electroreduction of Carbon Dioxide into Hydrocarbon Fuels. *Energy Environ. Sci.* **2010**, *3*, 1311.
(39) Peterson, A. A.; Nørskov, J. K. Activity Descriptors for CO_2 Electroreduction to Methane on Transition-Metal Catalysts. *J. Phys. Chem. Lett.* **2012**, *3*, 251−258.
(40) Shi, C.; Hansen, H. A.; Lausche, A. C.; Nørskov, J. K. Trends in Electrochemical CO_2 Reduction Activity for Open and Close-Packed Metal Surfaces. *Phys. Chem. Chem. Phys.* **2014**, *16*, 4720−4727.
(41) Nie, X.; Esopi, M. R.; Janik, M. J.; Asthagiri, A. Selectivity of CO_2 Reduction on Copper Electrodes: The Role of the Kinetics of Elementary Steps. *Angew. Chem. Int. Ed. Engl.* **2013**, *52*, 2459−2462.
(42) Nitopi, S.; Bertheussen, E.; Scott, S. B.; Liu, X.; Engstfeld, A. K.; Horch, S.; Seger, B.; Stephens, I. E. L.; Chan, K.; Hahn, C.; et al. Progress and Perspectives of Electrochemical CO_2 Reduction on Copper in Aqueous Electrolyte. *Chem. Rev.* **2019**, *119*, 7610−7672.
(43) Liu, X.; Xiao, J.; Peng, H.; Hong, X.; Chan, K.; Nørskov, J. K. Understanding Trends in Electrochemical Carbon Dioxide Reduction Rates. *Nat. Commun.* **2017**, *8*, 15438.
(44) Björketun, M. E.; Bondarenko, A. S.; Abrams, B. L.; Chorkendorff, I.; Rossmeisl, J. Screening of Electrocatalytic Materials for Hydrogen Evolution. *Phys. Chem. Chem. Phys.* **2010**, *12*, 10536−10541.
(45) Greeley, J.; Nørskov, J. K. Large-Scale, Density Functional Theory-Based Screening of Alloys for Hydrogen Evolution. *Surf. Sci.* **2007**, *601*, 1590−1598.
(46) Lu, G.; Evans, P.; Zangari, G. Electrocatalytic Properties of Ni-Based Alloys Toward Hydrogen Evolution Reaction in Acid Media. *J. Electrochem. Soc.* **2003**, *150*, A551.
(47) Greeley, J.; Jaramillo, T. F.; Bonde, J.; Chorkendorff, I. B.; Nørskov, J. K. Computational High-Throughput Screening of Electrocatalytic Materials for Hydrogen Evolution. *Nat. Mater.* **2006**, *5*, 909−913.

NOTE ADDED AFTER ASAP PUBLICATION

Originally published ASAP on November 12, 2020; updated November 17, 2020 with minor revisions in Results and Discussion.

https://dx.doi.org/10.1021/acs.jpcc.0c08832
J. Phys. Chem. C 2020, 124, 26344−26351